Spatially resolved below-gap emission in partially ordered $Ga_xIn_{1-x}P$ alloys

S. Smith,* A. Mascarenhas, S. P. Ahrenkiel, M. C. Hanna, and J. M. Olson
National Renewable Energy Laboratory, Golden, Colorado 80401, USA
(Received 3 July 2002; revised manuscript received 4 February 2003; published 10 July 2003)

We have examined the spatial variation in the photoluminescence (PL) of a series of partially ordered $Ga_xIn_{1-x}P$ ($x=0.52$) samples with order parameters ranging from $\eta\sim0.12$ to $\eta\sim0.49$ using low-temperature scanning confocal, scanning solid immersion lens, and scanning and fixed-aperture near-field microscopy with spatial resolution in the range from 200 nm to 0.7 μm. A wide variation in the characteristic low-energy emission band and the associated ultrasharp PL lines was observed for samples with similar ordering-related properties (e.g., η and domain size). In particular, not all samples exhibit sharp-line PL when examined using μ-PL techniques. In samples that do show these lines, near-field spectroscopic imaging is used to map their location in space with respect to the more slowly varying excitonic emission: no spatial correlation between the antiphase boundaries (APB's) which form in these alloys and the appearance of ultrasharp PL lines was observed. A correlation between the occurrence of ultrasharp PL lines and the presence of extended defects was found for some samples. Temperature-dependent and time-resolved studies show evidence of excitation transfer between a dense ensemble of discrete, localized states. The data suggest that models appealing solely to the properties of the APB in ordered GaInP cannot explain this emission, and that extended defects and/or impurities may play a more important role than previously thought.

DOI: 10.1103/PhysRevB.68.035310 PACS number(s): 78.66.Fd, 78.67.Hc, 71.55.Eq, 73.20.Hb

I. INTRODUCTION

$Ga_xIn_{1-x}P$ ($x\cong0.52$; hereafter referred to as GaInP) exhibits spontaneous $CuPt_B$-type ordering under certain growth conditions. This ordering manifests itself as a monolayer superlattice of the alternating layers $Ga_{(1+\eta)/2}In_{(1-\eta)/2}P/Ga_{(1-\eta)/2}In_{(1+\eta)/2}P$, oriented along $[111]_B$. Here η, known as the order parameter, is a statistical parameter describing the degree of ordering and can vary between 0 and 1. In practice, $\eta>0.5$ has proven difficult to achieve and thus only partial ordering is observed. The reduction in crystal symmetry upon ordering results in a band-gap reduction[1] and valence-band splitting[2] which are a function of η. Since η, and thus the material properties which depend upon it, can be tailored over a wide range by varying the growth conditions, ordered GaInP has attracted a great deal of interest for optoelectronic devices such as light-emitting diodes,[3] lasers,[4] and solar cells.[5] As such, this material system has been intensely studied and an extensive body of knowledge relating to ordered GaInP and spontaneous ordering has evolved (for a review, see Ref. 6 and 7).

One issue which has remained outstanding is the origin of the characteristic low-energy emission band which generally appears upon ordering. This emission has historically been associated with the submicron domain structure commonly observed in transmission-electron microscopy (TEM) studies: Uninterrupted ordering occurs only over length scales in the range of 100 nm–1.5 μm, depending on growth conditions, separated by antiphase boundaries (APB's), defined as a 180° phase shift in the {Ga-In-Ga-In...} stacking sequence between two uniformly ordered domains.[8] The orientation with respect to the ordering axis, morphology and exact composition of the APB's is sample dependent and at present poorly understood.[8,9]

This domain structure is not considered an intrinsic property of ordering, but rather, related to substrate and growth imperfections. However, it has been invoked on more than one occasion to explain experimental observations such as the origin of the low-energy photoluminescence (PL) band,[10–13] μs PL lifetimes,[11,14] and the ultrasharp quantum dotlike PL lines observed in μ-PL.[15–17] Relatively little work has been done to *directly* confirm these assertions and the physics of this emission remains unknown.

We present here an extensive study of the spatial variations in the low-temperature (typically 5 K) PL using scanning and fixed-aperture near-field microscopy, and confocal microscopy with and without a solid immersion lens (SIL). Ten samples with varying order parameters ($\eta\sim0.12$ to $\eta\sim0.49$) were examined. To avoid the possibility of studying anomalies associated with a particular growth chamber, samples from different growth facilities were also studied. We find that the strength and nature of the low-energy emission varies widely, often independent of ordering-related variables, suggesting that the origin of this emission may be due to nonordering-related defects or impurities.

II. EXPERIMENT

The series of samples studied are shown in Table I. All samples were grown on 6° miscut substrates oriented toward $[111]_B$, with the exception of sample 1, which was oriented toward $[111]_A$. Thus only single variant ordered samples were studied. The scanning confocal, near-field, and solid immersion lens measurements were made utilizing a low-temperature piezoelectric scanned-probe head described earlier[18] and retrofitted for the respective techniques, operating within a dynamic exchange gas cryostat at 5 K unless otherwise specified. The PL spectra taken were acquired using an 0.46-m single grating spectrometer (1800 lines/mm) and 2000×800 pixel charge-coupled device, with system resolution typically better than 100 μeV. For the time-resolved measurements, a fixed-aperture near-field technique

TABLE I. Sample number, growth facility, band gap, and order parameter for samples studied. A and B samples grown at National Renewable Energy Laboratory by separate metal-organic chemical-vapor deposition groups; C sample produced in Stuttgart. Sample 7 was studied in Ref. 19, sample 8 was studied in Ref. 13, sample 9 in Refs. 19 and 20, and sample 10 in Ref. 12.

Sample	Growth facility	E_g (ev)	η
1	A	1.998	0.12
2	B	1.975	0.25
3	A	1.959	0.30
4	B	1.931	0.39
5	A	1.927	0.40
6	A	1.923	0.41
7	B	1.923	0.41
8	B	1.915	0.43
9	B	1.906	0.45
10	C	1.887	0.49

was used, wherein an array of 0.2–μm apertures were fabricated on an aluminum film deposited on sample 9 in Table I; this sample was studied in Ref. 19. Resonant excitation of ultrasharp below-gap PL lines was achieved using a synch-pumped dye laser producing tunable 5-ps pulses with $\sim$0.6-meV bandwidth. Time-resolved PL (TRPL) was measured using time-correlated single-photon counting.

III. RESULTS

A. Confocal/SIL study

The low-temperature scanning μ-PL apparatus used was described in a previous paper, and typically achieves a spatial resolution of 0.7 μm.[18] For the SIL measurements, the following modifications were made: (i) A hemispherical solid immersion lens[21](material LASFN9, $n=1.85$) was placed in contact with the sample and used in conjunction with an aspheric lens to give a numerical aperture of 1.02, corresponding to a diffraction-limited excitation spot size of 325 nm and (ii) the confocal imaging geometry was relaxed to increase the signal collection efficiency. In practice, the spatial resolution of the SIL system was limited to roughly 500 nm, derived by examining the full width at half maximum (FWHM) of various features in the spatial-spectral images. The scan range in both lateral dimensions was fixed at 5.5 μm, unless otherwise stated.

All samples listed in Table I were examined at $T=5$ K with the above-described apparatus, and it was generally discovered that not all samples show sharp lines when examined using μ-PL techniques. To illustrate this point, we compare here two highly ordered samples with similar ordering-related properties: Both have large domain sizes (greater than 0.5 μm) and therefore similar domain boundary density; both are strongly ordered, with similar order parameters ($\eta=0.45$ and 0.43); the first sample (sample 9 in Table I) showed a large number of sharp lines [hereafter referred to as low-energy lines (LEL's)], while the other (sample 8 in Table I) showed none. By holding the ordering-related variables

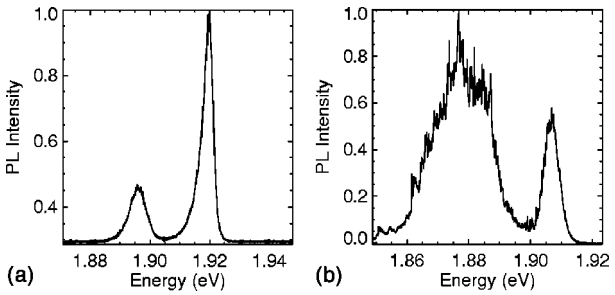

FIG. 1. (a) and (b): Typical PL spectrum taken with SIL apparatus under identical conditions (I$\approx$250 W/cm^2), for each sample (8 and 9, left to right).

constant (that is, η and the domain size), we compare here the μ-PL measurements and illustrate the dramatic differences in the nature of the low-energy emission and associated LEL's, which appear to be independent of η and the domain size.

Comparing the spectra shown in Figs. 1(a) and 1(b), it can be seen that sample 9 exhibits a much stronger, broader, low-energy emission, and, as will be seen by examining the spatial-spectral data that follows, a much higher density of LEL's. Given that the density of APB's in these two samples is approximately equal, either the nature of the electronic states associated with the APB in sample 9 is very different from that of sample 8, or some other property of this sample gives rise to the many sharp lines observed. While these samples are similar with respect to ordering-related variables, several differences do exist which may be important. First, TEM micrographs of sample 9 showed many edge dislocations (the areal density in plain-view images was $\sim 10^8$ cm^{-2}), but no measurable dislocations were found in sample 8.[22] The presence of crystalline defects was also confirmed by x-ray-diffraction measurements, which yielded FWHM's of 55 and 28 mRad for samples 9 and 8, respectively. Other differences include 3 vs 4 μm/hr growth rate, and n-doped vs semi-insulating substrates.

Figure 2 shows a PL spectrum taken from the collection of spectra ($\sim$1000 per image) for sample 9 using the SIL system. A PL intensity map formed at the energy of the intense sharp line seen in the spectra is shown in the inset. This spectra was acquired in the center of the the bright spot

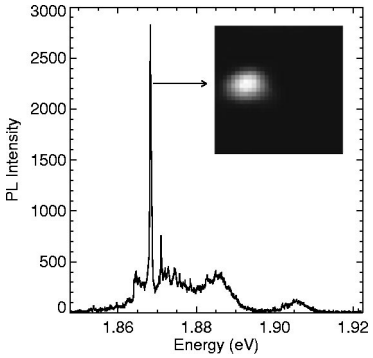

FIG. 2. PL spectrum taken at center of bright region of PL map shown in inset (scan area 5.5$\times$5.5 μm^2) for sample 9 in Table I. PL image acquired at 5 K with SIL.

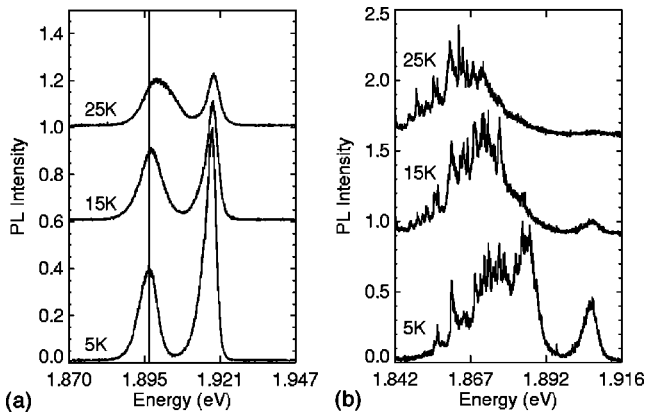

FIG. 3. Temperature dependence of the low-energy band for samples 8 (a) and 9 (b), normalized to the maximum PL intensity at 5 K for each sample (spectra offset for clarity).

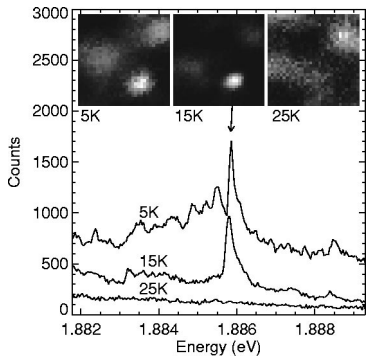

FIG. 4. Expanded energy scale of low-energy region of PL in sample 9 at $T=5$ K, $T=15$ K, and $T=25$ K. Inset shows the spatial intensity map formed at the energy of the central spike (marked by an arrow). All spectra were taken in the central region of the bright region most easily seen in the $T=15$ K image. At 25 K, this bright region disappears and the spectrum appears flat, indicating that this localized state has ionized.

shown in the PL map. At lower excitation powers ($P \approx 13$ nW, estimated intensity ≈ 7 W/cm^2) carriers accumulate at the energetically narrow ($\Delta E \sim 400$ μeV) line shown in the spectra, thus we see the strong intensity contrast in the PL map. This particular line has a much stronger emission than energetically neighboring states. By examining the spatial PL maps formed throughout the measured spectrum, multiple such LEL's can be identified and localized within the imaging resolution.

The spatial frequency for the occurrence of these stronger LEL's (roughly $1/\mu$m^2) is in reasonable agreement with the dislocation density, and a similar association was found for sample 7. Emission localized and concentrated at crystalline defects has been observed in cathodoluminescence studies of AlGaAs barrier layers in single quantum wells,[23] and time-resolved PL studies have shown that dislocations act as effective recombination centers at GaInP/GaAs heterojunctions.[24] Since dislocations perturb the binding energy in their immediate vicinity, impurities and point defects tend to find energetically favorable sites nearby and thus tend to getter at these sites. This could explain the extremely bright LEL depicted in Fig. 2: Photoexcited carriers within the low-energy band could be trapped and concentrated near crystalline defects, but would still exist throughout the bulk of the sample, accounting for the substantial background.

Such a picture implies the coexistence of discrete, strongly localized states with a quasicontinuum of below-gap transitions, which together comprise the low-energy emission. Figure 3(a) shows the temperature dependence of the μ-PL spectra taken at the center of the 5.5×5.5–μm^2 region of sample 8 while the temperature was varied from 5 to 25 K (the resulting drift in the image plane was negligible over that temperature range). The low-energy emission band is seen to shift to higher energy with increasing temperature with a pronounced asymmetric broadening toward higher energy. This behavior can be explained by assuming a continuum of states occupied according to thermal statistics. Figure 3(b) shows an identical measurement of sample 9. Here the low-energy band has many sharp peaks, which tend to decrease in energy as the temperature is increased. This fundamentally different behavior can be explained by assuming a high density of localized, discrete states: With the addition of thermal energy, localized excitons can hop out of local potential minima and subsequently scatter into available lower-energy states.

This is directly observed in the series of spectra taken from sample 9, shown in Fig. 4. The expanded energy-scale spectra taken in the center of the bright spot in the lower-right side of the PL images (shown in the inset) are displayed as a function of temperature. The spectra show a sharp decrease in intensity with increasing temperature, and a slight shift to lower energy, presumably due to the weak temperature dependence of the band-gap energy in this temperature range. An arrow in the spectra indicates the energy at which the PL maps were formed. The spectra are naturally stacked along the vertical axis due to the increase in nonradiative recombination with increasing temperature. The indicated peak is diminished with increasing temperature and extinguished in the spectrum taken at 25 K. Examining the PL maps, increasing temperature from left to right, there are three localized emission centers observable in the 5-K image. In the 15-K image the two upper localized emission sites have been greatly suppressed, causing the localized center on the lower-right side to appear with more contrast. In the third PL image, the localized transition in question has disappeared, in concert with the LEL in the spectra. The LEL in question has ionized with the addition of ~ 2 meV of thermal energy. This value is not atypical, although not all isolated lines observed ionized over the temperature ranges studied; presumably this value would depend on the microscopic details at a given site. This observation is consistent with the above interpretation of the temperature dependence of the low-energy emission in sample 9. The observations in both samples could be explained in terms of impurities and possibly alloy fluctuations with the assumption that the presence of crystalline defects promotes the formation of localized states, in which case the absence of these defects in sample 8 and their relative abundance in sample 9 could account for the remarkably different temperature dependence.

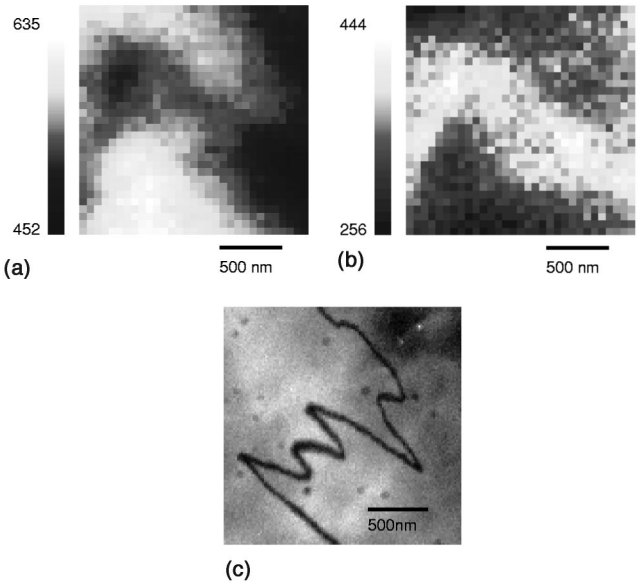

FIG. 5. (a) Integrated PL intensity of excitonic emission (gray scale is averaged intensity, in counts/sec), measured using near-field spectroscopic imaging. (b) PL intensity map formed near peak of low-energy emission band. (c) 1.8×1.8 μm^2 plain-view TEM image showing typical APB in this sample.

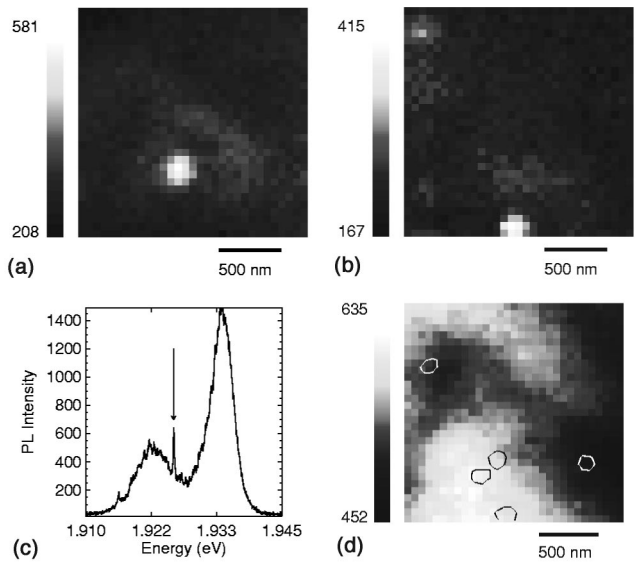

FIG. 6. (a): PL intensity map at specific energy ($\sim$1.192 57 eV) indicated by an arrow in the spectrum shown in (c). (b) Similarly localized transition at $\sim$1.928 eV. (c) PL spectrum taken at center of bright region in PL map shown in (a). (d) Contours overplotted on PL intensity map of Fig. 5 (a); each contour bounds an isolated ''quantum dotlike'' transition.

B. Near-field spectroscopy

The above-mentioned scanning microscopy system was retrofitted as a near-field microscope by attachment of a custom-designed near-field fiber tip assembly, consisting of a tapered fiber tip of the variety reported by Betzig *et al.*[25,26] held in a piezoelectric dither assembly. PL was excited and collected in shared-aperture mode, using a nominal 200-nm diameter aperture at the apex of the tapered fiber probe.

Figure 5(a) shows an image of sample 5 taken with the scanning near-field apparatus at $T=5.0$ K. The scan area is 1.8–μm square, and the spatial resolution was $\sim$200 nm, verified by measuring the FWHM of multiple features in the images formed at various energies. The image shows the averaged integrated intensity of the excitonic emission [the high-energy peak in the spectrum of Fig. 6(c)]. Inspecting the image, a decrease in excitonic PL intensity is observed to thread across the image plane, which is similar to the wandering domain boundaries observed in the plain-view TEM image of this sample, shown in Fig. 5(c). Inspection of the PL image formed near the peak of the low-energy emission band, shown in Fig. 5(b), directly anticorrelates with the image of Fig. 5(a).

It is important to note here that the low-energy emission generally appears throughout the sample and is only relatively stronger (by a factor of about 2) at the boundary region shown in Fig. 5(b). In a statistical study of over 200 subwavelength apertures formed on large-domain GaInP samples, the authors of Ref. 20 also reported that this emission was omnipresent. It is not certain that the observed boundary has the same origin as the APB's seen in TEM images, but the resolution of these measurements is sufficiently high to easily resolve any emission localized to the APB. From these observations, one can conclude that the below-gap emission band cannot be exclusively associated with the APB's observed in this material.

Within the low-energy near-field emission spectra taken in sample 5 were interdispersed many of the LEL's discussed above. For instance, the transition indicated by the arrow in Fig. 6(c) has an estimated FWHM of $\sim$300 μeV. Such transitions have been investigated using nonscanning aperture near-field techniques[15,16,20] and indeed show many of the spectral signatures of a $0-d$ state. Here, we spatially localize several of these ''quantum dotlike'' transitions with respect to the more slowly varying excitonic emission. When examining the spatial maps at specific energies within the spectrum (which is taken at every point in the image plane), an ''island'' which is much brighter than any other feature in the image plane will occur. If one examines the spectrum taken at the spatial location of the ''island,'' one of the aforementioned LEL's will be centered at the energy at which the image was formed, and thus a one-to-one correspondence between the transition and the spatial location can be made.

Such an image is shown in Fig. 6(a), and the corresponding energetically narrow transition is indicated by the arrow in Fig. 6(c). Several (five) of these ''quantum dotlike'' transitions have been localized in this way; Fig. 6(d) shows contours which bound their location in space overlaid on the PL intensity map of Fig. 5(a). The two right-most black contours in the lower-center region of the figure localize the indicated transitions shown in the PL maps of Fig. 6(a) and 6(b). Inspecting the figure, we see that three of these transitions can be localized within a region of uniform excitonic emission. Similarly, the two white contours appear in the boundary region mapped out in Fig. 5(b). Thus no spatial correlation between the presence of the LEL's and the low-energy band is observed. In light of the above discussion, there is simi-

larly no observed correlation between the LEL's and the APB. LEL's were observed in the energy range spanning the low-energy band and extending into the excitonic emission peak and even well above the band gap (on rare occasion), further suggesting that these two emissions have distinct origins.

C. Fixed-aperture near-field study

Reference 19 presents a μ-photoluminescence excitation (μ-PLE) study of samples 7 and 9 using a nonscanning near-field technique,[27] wherein submicron (250 nm) apertures were fabricated in an otherwise opaque aluminum film deposited on the samples studied. It was observed that many of the LEL's in those samples showed energetically narrow absorption peaks (as narrow as 100 μeV) which did not correspond to any LEL in the PL spectrum. Furthermore, the same absorption peak would appear in the μ-PLE spectra of different LEL's (within the same aperture), without any cross excitation among the different LEL's. The possible explanation of these ''dark'' absorption peaks put forth in that paper was that energetically and spatially neighboring localized states undergo exciton transfer via tunneling. In this picture, localized emission centers from which lower-energy LEL's originate couple strongly to a neighboring site and effectively quench the PL at this site. This transfer must take place on a time scale less than the PL lifetime of the LEL, typically on the order of a nanosecond. To test this picture, we resonantly excite at these narrow-band absorption lines and subsequently time-resolve the PL at the various lower-energy LEL.

In order to resonantly excite these narrow-line states, a picosecond synchronously pumped dye laser was tuned in resonance with the absorption peaks observed in μ-PLE measurements of sample 9, discussed in detail in Ref. 19. The energy bandwidth of the $\sim$5-ps pulses was roughly 600 μeV, and the pulse repetition rate was varied between 25 and 38 MHz, to optimize the signal-to-noise ratio. Typically 1–5-μW average power over the energy bandwidth of the absorption resonance was used to excite observable PL at energetically neighboring states within a given aperture. It was generally observed that the absorption was weaker for pulsed vs continuous excitation.

Figure 7(a) shows a typical TRPL time trace for a single LEL 6.3 meV below the excitation energy. A delay in the PL decay is demonstrated by the $\sim$210-ps plateau shown in the figure. This delay is indicative of the excitation transfer described above. Select apertures which showed strong narrow-band absorption resonances were examined. Figure 7(b) shows the observed PL delay time as a function of the energy offset between the excitation and the observed LEL, the lower limit being set by the time resolution of the time-correlated single-photon counting apparatus used (50 ps) and the rejection limit of the spectrometer. It is evident and intuitively reasonable that the observed delay increases monotonically as a function of energy offset. The transfer process is likely an incoherent, multistep process involving multiple tunneling events and subsequent relaxation by acoustic-phonon emission. Such a picture implies a high density of

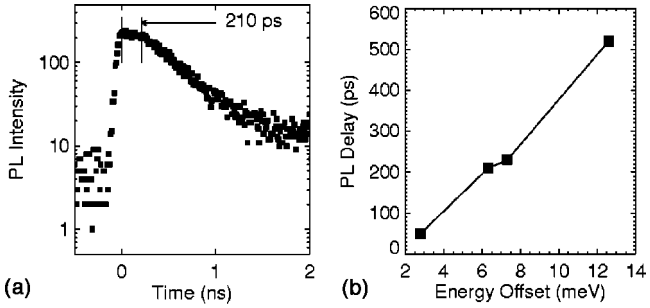

FIG. 7. (a) Resonantly excited TRPL detected at LEL 6.3-meV below absorption resonance. A 210-ps delay in PL decay attributed to exciton transfer from spatially neighboring localized states is shown. (b) PL delay times plotted as a function of energy offset for select LEL.

localized states. In view of the inherent disorder in this system and the lack of knowledge concerning the below-gap electronic states, it is difficult to describe the process in more detail. The measurements support the mechanism for exciton transfer among spatially neighboring LEL's proposed in Ref. 19.

IV. DISCUSSION

In Sec. III A, we compared two highly ordered samples with similar order parameter and domain size. In spite of these similarities, the behavior of the low-energy emission band with temperature was dramatically different, with one sample showing a high density of localized states, the other only delocalized states. Thus, at least two types of transitions can appear in the low-energy emission of this material, in agreement with the conclusions of the magneto-PL in Ref. 16, where these two types of emission (labeled ''LEL'' and ''LEB'' in that work) showed a quadratic and linear diamagnetic shift, respectively. However, in this work, we find a great disparity in the number of LEL's observed, while the order parameter and domain size are held constant. We thus find no correlation between the number of LEL's and the density of APB's. This is reinforced by the low-temperature near-field PL imaging results shown in Sec. III B, where again no correlation between the LEL's and APB's was observed. Furthermore, the emission of the delocalized low-energy band appeared omnipresent in the near-field PL images. We therefore conclude that the origin of this band need not be tied solely to the APB, since these are highly localized and sparse for that sample.

Reference 16 proposed that the LEL's arise from quantum confinement within the APB, envisioned as an InP double layer, embedded in an ordered-GaInP matrix. This microstructure was investigated theoretically in Ref. 17, where it was proposed that hole confinement in the APB gives rise to both the broad low-energy emission band and the LEL. From the above discussion, we find no evidence suggesting that either of these emissions originate from this proposed microstructure. The appearance of the APB indicates a change in phase of the stacking sequence between two ordered domains. As illustrated in Fig. 8, it is not necessary that this change in phase occur along the ordering direction, and, as

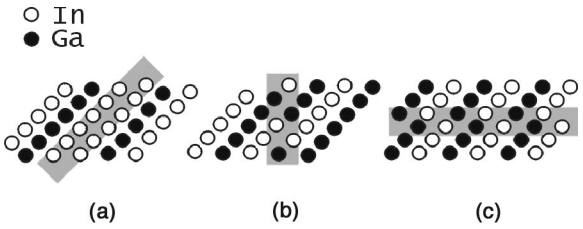

FIG. 8. Schematic of ordered Ga(In)-rich planes when viewed along $\langle 110 \rangle$ (perpendicular to ordering axis $\langle 1\bar{1}1 \rangle$). (a) Antiphase boundary (APB, highlighted in gray) resulting from In(Ga)-In(Ga) double layer. (b) APB resulting from vertical phase shift. (c) APB resulting from horizontal phase shift.

mentioned previously, the orientation and composition of the APB's can vary widely.[9] While we can not exclude electronic states associated with this microstructure, the evidence presented here suggests that this is not a general description of either the LEL or the low-energy emission band.

In μ-PLE measurements,[19] it was shown that the LEL's typically have ultranarrow absorption resonances. By exciting select LEL's resonantly, and time resolving the emission of spatially and energetically neighboring LEL's, we observed exciton transfer among the LEL's on time scales of a few 100 ps. The transfer times were observed to depend monotonically on the energy offset of the absorbing and emitting states, giving evidence that the transfer time is primarily determined by acoustic-phonon emission. This suggests a high density of localized states, coupled by tunneling. The temperature dependence of the localized emission of sample 9 discussed in Sec. III A also supports this picture, where thermal ionization and a shift to lower energies with increasing temperature was observed for select LEL's.

Extremely weak thermal broadening, ultranarrow linewidths, and efficient exciton transfer among a dense ensemble of localized states associated with impurities have been observed in GaP:N (Refs. 28 and 29) and GaInP:N.[30] The fact that large differences in the nature and strength of the low-energy emission were observed for samples with similar ordering-related properties (e.g., η and domain size) and the observed correlation of the LEL with dislocation density suggests that extended defects and/or impurities may play a role in the formation of the LEL's observed in GaInP. The fact that similar LEL's are not typically observed in disordered GaInP or other ternary alloys such as AlGaAs suggests that ordered GaInP is particularly sensitive to such defects, and that further studies are needed to determine the origins of both the low-energy band and the LEL's.

V. SUMMARY

We examined the spatial variations in the low-energy emission in a series of ordered-GaInP samples with order parameters in the range $\eta \sim 0.12-0.49$. We find large variations in the strength and constituents of this emission between samples: Signatures of localized or delocalized emission can be found to dominate this band, independent of the order parameter or domain size. Near-field spectroscopic imaging was used to localize the ultrasharp quantum dotlike LEL with respect to the more slowly varying excitonic emission and low-energy band, showing no evidence that these transitions are localized to the antiphase boundaries (APB's) commonly observed in this material. These observations suggest that the origin of the below-gap emission remains unexplained, and that models appealing solely to the properties of the APB cannot account for this emission. Time-resolved PL measurements with submicron apertures in patterned samples reveal that exciton transfer takes place between LEL's within 50–500 ps, increasing monotonically with the energy difference between the absorbing and emitting states, most likely involving tunneling within a dense ensemble of localized states. Temperature-dependent PL measurements also support this picture. A correlation between the occurrence of the LEL's and the presence of extended defects was found for some samples. One possible explanation for this association is that the presence of extended defects promotes the formation of localized states by gettering impurities or influencing alloy fluctuations.

ACKNOWLEDGMENTS

This research was supported by the Office of Energy Research (Material Science Division) of the U.S. Department of Energy under Contract No. DE-AC36-83CH10093.

*Email address: steven_smith@nrel.gov

[1] A. Gomyo, T. Suzuki, and S. Iijima, Phys. Rev. Lett. **60**, 2645 (1988).
[2] A. Mascarenhas, S. Kurtz, A. Kibbler, and J. M. Olson, Phys. Rev. Lett. **63**, 2108 (1989).
[3] K. H. Huang, C. P. K. J. G. Yu, R. M. Fletscher, T. D. Osentwski, L. J. Stinson, M. G. Craford, and A. S. H. Liao, Appl. Phys. Lett. **61**, 1045 (1992).
[4] H. Fujii, Y. Ueno, A. Gomyo, K. Endo, and T. Suzuki, Appl. Phys. Lett. **61**, 737 (1992).
[5] K. A. Bertness, S. R. Kurtz, D. J. Friedman, A. E. Kibbler, C. Kramer, and J. M. Olson, Appl. Phys. Lett. **65**, 989 (1994).
[6] *Spontaneous Ordering in Semiconductor Alloys*, edited by A. Mascarenhas (Kluwer Academic/Plenum, New York, 2002).
[7] *Self-Organized Processes in Semiconductor Alloys*, edited by A. Mascarenhas, D. Follstaedt, T. Suzuki, and B. Joyce (Materials Research Society, Pittsburgh, 1999).
[8] S. P. Ahrenkiel, in *Spontaneous Ordering in Semiconductor Alloys* (Kluwer Academic/Plenum, New York, 2002), Chap. 7.
[9] S. P. Ahrenkiel and M. C. Hanna, Appl. Phys. Lett. **79**, 1781 (2001).
[10] M. C. Delong, P. C. Taylor, and J. M. Olson, Appl. Phys. Lett. **57**, 620 (1990).
[11] J. E. Fouquet, V. M. Robbins, J. Rosner, and O. Blum, Appl. Phys. Lett. **57**, 1566 (1990).
[12] P. Ernst, C. Geng, G. Hahn, F. Scholz, H. Schweizer, F. Phillup, and A. Mascarenhas, J. Appl. Phys. **79**, 2633 (1996).
[13] H. M. Cheong, A. Mascarenhas, S. P. Ahrenkiel, K. M. Jones, J. F. Geisz, and J. M. Olson, J. Appl. Phys. **83**, 5418 (1998).

[14] P. E. Ernst, C. Geng, F. Scholz, and H. Schweizer, Phys. Status Solidi A **193**, 213 (1996).
[15] U. Kops, R. G. Ulbrich, M. Burkard, C. Geng, F. Scholz, and M. Schweizer, Phys. Status Solidi A **164**, 459 (1997).
[16] U. Kops, P. G. Blome, M. Wenderoth, R. G. Ulbrich, C. Geng, and F. Scholz, Phys. Status Solidi A **61**, 1992 (2000).
[17] T. Mattila, S.-H. Wei, and A. Zunger, Phys. Rev. B **83**, 2010 (1999).
[18] S. Smith, H. M. Cheong, B. D. Fluegel, J. F. Geisz, J. M. Olson, L. L. Kazmerski, and A. Mascarenhas, Appl. Phys. Lett. **74**, 706 (1999).
[19] B. Fluegel, S. Smith, Y. Zhang, A. Mascarenhas, J. F. Geisz, and J. M. Olson, Phys. Rev. B **65**, 115320 (2002).
[20] H. M. Cheong, A. Mascarenhas, J. F. Geisz, J. M. Olson, M. W. Keller, and J. R. Wendt, Phys. Rev. B **57**, R9400 (1998).
[21] S. M. Mansfield and G. S. Kino, Appl. Phys. Lett. **57**, 2615 (1990).
[22] TEM images of sample 8 can be found in Ref. 12; images of sample 9 are unpublished.
[23] D. Araújo, G. Oelgart, J. D. Ganière, and F. K. Reinhart, J. Appl. Phys. **74**, 1997 (1993).
[24] M. Müllenborn, K. Matney, M. S. Goorsky, N. M. Gaegel, and S. M. Vernon, J. Appl. Phys. **75**, 2418 (1994).
[25] E. Betzig, J. K. Trautman, T. D. Harris, J. S. Weiner, and R. L. Kostelak, Science **251**, 1468 (1991).
[26] H. F. Hess, E. Betzig, T. D. Harris, L. N. Pfeiffer, and K. W. West, Science **264**, 1740 (1994).
[27] D. Gammon, E. S. Snow, B. V. Shanabrook, D. S. Katzer, and D. Park, Science **273**, 5271 (1996).
[28] D. E. McCumber and M. D. Sturge, J. Appl. Phys. **34**, 1682 (1963).
[29] P. J. Wiesner, R. A. Street, and H. D. Wolf, Phys. Rev. Lett. **35**, 1366 (1975).
[30] H. Mariette, J. A. Kash, D. J. Wolford, and A. Marbeuf, Phys. Rev. B **31**, 5217 (1985).